Experimental Investigation of Subsonic Turbulent Boundary Layer Flow Over a Wall-Mounted Axisymmetric Hill

James H. Bell, James T. Heineck, Gregory Zilliac, Rabindra D. Mehta, Kurtis R. Long
MS 260-1 NASA Ames Research Center
Moffett Field, California, 94035
UNITED STATES

James.H.Bell@nasa.gov

ABSTRACT

An important goal for modern fluid mechanics experiments is to provide datasets which present a challenge for Computational Fluid Dynamics simulations to reproduce. Such "CFD validation experiments" should be well-characterized and well-documented, and should investigate flows which are difficult for CFD to calculate. It is also often convenient for the experiment to be challenging for CFD in some aspects while simple in others. This report is part of the continuing documentation of a series of experiments conducted to characterize the flow around an axisymmetric, modified-cosine-shaped, wall-mounted hill named "FAITH" (Fundamental Aero Investigates The Hill). Computation of this flow is easy in some ways – subsonic flow over a simple shape – while being complex in others – separated flow and boundary layer interactions. The primary set of experiments were performed on a 15.2 cm high, 45.7 cm base diameter machined aluminum model that was tested at mean speeds of 50 m/s (Reynolds Number based on height = 500,000). The ratio of model height to boundary later height was approximately 3. The flow was characterized using surface oil flow visualization, Cobra probe to determine point-wise steady and unsteady 3D velocities, Particle Image Velocimetry (PIV) to determine 3D velocities and turbulence statistics along specified planes, Pressure Sensitive Paint (PSP) to determine mean surface pressures, and Fringe Imaging Skin Friction (FISF) to determine surface skin friction magnitude and direction. A set of pathfinder experiments were also performed in a water channel on a smaller scale (5.1 cm high, 15.2 cm base diameter) sintered nylon model. The water channel test was conducted at a mean test section speed of 3 cm/s (Reynolds Number of 1500), but at the same ratio of model height to boundary layer thickness. Dye injection from both the model and an upstream rake was used to visualize the flow. This report summarizes the experimental set-up, techniques used, and data acquired. It also describes some details of the dataset that is being constructed for use by other researchers, especially the CFD community.

1.0 NOMENCLATURE

CAD = Computer-Aided Design
C_f = skin friction coefficient
C_p = pressure coefficient
D = model base diameter
FML = Fluid Mechanics Laboratory
h = model height above baseline
H = model maximum height

P = total pressure
p = static pressure
q = dynamic pressure
R = model base radius
RPM = revolutions per minute
r = radial distance from model centroid
Re_H = Reynolds Number based on model height
TKE = turbulent kinetic energy, = $[\overline{(u')^2} + \overline{(v')^2} + \overline{(w')^2}]/2$
u = instantaneous streamwise velocity component (positive downstream); $u = \bar{u} + u'$
v = instantaneous vertical velocity component (positive upwards); $v = \bar{v} + v'$
V_{mean} = time-averaged facility velocity at test section centerline
w = instantaneous cross-stream velocity component (positive rightwards); $w = \bar{w} + w'$
$\bar{u}$ = time-averaged streamwise velocity component (positive downstream)
$\bar{v}$ = time-averaged vertical velocity component (positive upwards)
$\bar{w}$ = time-averaged cross-stream velocity component (positive rightwards)
u' = fluctuating streamwise velocity component (positive downstream)
v' = fluctuating vertical velocity component (positive upwards)
w' = fluctuating cross-stream velocity component (positive rightwards)
x = distance downstream of model centroid
y = distance above tunnel floor
z = distance right of model centroid
δ = boundary layer thickness (height at which velocity = 99% of free stream value)

1.0 INTRODUCTION

Subsonic flow around a wall-mounted bump or hill protruding through the boundary layer (figure 1-1) can create a variety of interesting features including unsteady vortical flow separation and reattachment as well as necklace or horseshoe vortices. The ability to characterize such features is of fundamental importance in solving variety of design optimization and analysis problems. In particular, such a flow field turns out to be a perfect candidate for the development and validation of Computational Fluid Dynamics (CFD) methods. The main reason for this is that the hill model can generate a flow field with almost all the complex features that are generally challenging for CFD methods namely, pressure gradient and curvature effects together with three-dimensional (3-D) boundary layer separation and reattachment. Previous experimental studies (references 1 through 9) investigated the subsonic flow characteristics of an axisymmetric hill immersed in a boundary layer. Reynolds number is a factor in the flow around wall-mounted hills; Hunt *et. al.* [1] show that re-attachment of the separated flow downstream of the hill's crest only occurs when the boundary layer is turbulent, as diagrammed in figure 1-2. Thus immersion in a turbulent wall boundary layer results in flows which are of greater interest for CFD studies. References 6 through 9 used a variety of experimental techniques, including Laser Doppler Velocimetry (LDV), Hot-Wire Anemometry (HWA), and piezoresistive pressure transducers, to investigate both on- and off-surface parameters associated with the separated flow arising from an axisymmetric hill immersed in a turbulent boundary layer flow. In 2006, the turbulence modeling and simulation community (reference 10) set the axisymmetric hill or bump immersed in a subsonic boundary layer as a test case worthy of further computational study. As a result, several computational Large Eddy Simulation (LES) investigations (references 11 through 14) used these experimental studies to help assess the capabilities of various computational techniques that might be employed to help gain insight into the physical wake phenomena associated with separating and reattaching flows about such shapes. This work persuaded the authors that a well-characterized experimental investigation of the flow over a wall-mounted axisymmetric hill immersed in a subsonic boundary layer would be useful for CFD validation purposes.

The main objective of the present study was to generate an experimental database with well-documented inlet and boundary conditions that will enable an assessment of our ability to predict flow separation location and complex flow behavior in the separated region over a model with simple geometry. The approach was to conduct a set of wind tunnel and water channel experiments on a small wind tunnel model known as FAITH (Fundamental Aero Investigates The Hill; figure 1-3) that would contribute towards understanding of the separating and reattaching flow characteristics associated with a wall-mounted axisymmetric hill immersed in a subsonic boundary layer.

Three model parameters were considered to be of significance to the FAITH project: the generating function for the shape, the ratio of model height to base radius (H/R), and the ratio of model height to boundary layer thickness (H/δ). In addition it was considered important that the flow remain qualitatively similar over a large Reynolds number range and that the model should protrude through a fully-developed turbulent boundary layer. (It was expected that these last two factors would simplify the CFD problem.) The cosine function shape was chosen to eliminate surface discontinuities and thus make the model easy to grid for CFD simulation. The height-to-radius ratio was chosen to reliably induce flow separation over the downstream side of the model. Based on the authors' engineering judgment $H/R = 1/3$ appeared to be appropriate and this proved to be the case. The height-to-boundary layer thickness ratio was set partially by facility considerations. It was desired to have the model height and boundary layer thickness be the same order of magnitude, as this would provide the most interesting problem for CFD. In addition it was desired to do the majority of the tests in the Fluid Mechanics Laboratory's Test Cell #2 wind tunnel, which has a wall boundary layer thickness of about 5 cm. Ideally, the model would be as large as possible for the wind tunnel because the flow over a large model could be characterised in finer spatial detail. At this point the Fluid Mechanics Laboratory's water channel facility proved very valuable. Within the water channel models can be placed at different positions along a splitter plate corresponding to different values of boundary layer thickness; thus the ratio H/δ can be easily varied. A small model was quickly fabricated and equipped for dye flow visualization. Multiple runs at varying distances along the splitter plate indicated that $H/\delta = 3$ resulted in a good interaction between the model and boundary layer while allowing a reasonable model size.

Table 1-1: FAITH Project Summary

Model and Size	Vmean (m/s); Re_H	H/δ	Test Technique	Measurements/ Documentation	Measurement Location Description (Center of Model Base: X=Y=Z=0)	Measurement Extents
SLS Nylon; R = 7.6 cm H =5.1 cm	0.03; 3E3	3	Water Channel Dye Flow Visualization	Video, Still Images	Overall Flowfield Centerline Laser Sheet	0< x/H < 6; y=0, 0<z/H<2 0< x/H < 6; y=0, 0<z/H<2
Aluminum; R = 22.9 cm H = 15.2 cm	50.3; 5E5	3	Wind Tunnel Oil Flow Visualization	Still Images	Entire Surface of Model	0< x/H < 6; y=0, 0<z/H<2
			PSP	Mean Surface Pressures	Entire Surface of Model	r/R < 1
			PIV	4000 samples@ 2 hz; 3D Velocity Statistics	8 Longitudinal-Vertical planes	0<x/H < 6; y=--2, 0, 2,3,4,4.75,6,7; 0<z/H<2
			Cobra Probe	6 sec samples @1250 hz of 3D velocity data;	1 centerline plane (500 points) 7 vertical-lateral planes (500 points)	0< x/H < 6; y=0, 0<z/H<2 0< x/H < 6; y=0, 0<z/H<2
			FISF	Mean Skin Friction Magnitude and Direction	Entire Surface of Model	r/R < 1
			Discrete Surface Pressures	Mean Surface Pressures	Entire Surface of Model	12 discrete locations

Having established the parameters governing the model shape and size, the project then employed a battery of experimental techniques to measure significant on-and off-surface parameters, as well as inlet and outlet flow conditions. Experimental techniques were chosen both for availability to the authors and to acquire as many possible parameters of interest. Thus surface measurements included oil flow to characterize qualitative surface features, Pressure-Sensitive Paint (PSP) and pressure taps to establish surface pressures, and Fringe Imaging Skin Fruction (FISF) to determine the skin friction distribution. Off-body velocity measurements were made with a Cobra probe to obtain three-component fluctuating velocities, and with Particle Image Velocimetry (PIV) as an

independent non-intrusive source of three-component velocities, turbulence characteristics, and spatial cross-correlations.

This report summarizes the data acquired to this point, and also describes the dataset that is being made available for use by researchers. The authors have previously presented a more limited discussion of the FAITH dataset [15] and expect to provide a more detailed description of the results in future work.

2.0 FACILITIES AND MODELS

2.1 Wind Tunnel Facility

The NASA Ames Fluid Mechanics Lab's (FML's) Test Cell #2 facility (figure 2-1) was employed for this effort. It is an open-circuit indraft wind tunnel using flow supplied by a centrifugal compressor located downstream of the test section. A detailed description of the facility is available in ref 16. The facility compressor runs at constant RPM; mass flow (and hence, speed) through the test section is controlled by means of a variable-area sonic throat. Flow travels from the lab into the bellmouth, through a honeycomb and 3 screens, and into a 9:1 contraction. Downstream of the contraction is the wind tunnel test section, which is approximately 1.22 m wide, 0.81 m tall, and 3.05 m long. The maximum centerline mean velocity in the test section is 52 m/s, corresponding to a Reynolds Number of approximately 3.2 million per meter. The minimum achievable velocity, due to pressure recovery limits, is 12 m/s. The free-stream turbulence intensity (TI) and boundary layer height (δ) at the midpoint of the empty test section are approximately 0.13% and 3.8 cm, respectively.

The test section side walls are constructed from acrylic panels, hinged at the top, which allow maximum optical and physical access to the model. Above the test section is a 1.22 m × 0.81 m × 3.05 m long plenum designed to accommodate flow measurement instruments. The acrylic ceiling between the tunnel and plenum is not airtight, and thus the plenum is maintained at test section static pressure during operation. Traversing probes mounted in the plenum can access the test section through temporary slots in the ceiling of the tunnel while minimizing flow disturbances. The test section floor is made from replaceable sections of marine-grade plywood which can be customized to fit the needs of individual tests. A CAD geometry model of the facility is available for use in simulations. The CAD model is based on the facility design documents with some updates for as-built measurements based on spot checks.

2.2 Wind Tunnel Facility Control Instrumentation

During wind tunnel testing, existing facility instrumentation was used for control and speed measurement. MKS Instruments 698A Barotron differential pressure transducers were employed to measure inlet and test section dynamic pressures, and a United Sensor pitot-static thermocouple was employed to measure test section dynamic pressure and temperature, which were used in speed computations. The FML's standard Labview-based wind tunnel instrumentation system (BDAS) was employed to control tunnel conditions and record data for the wind tunnel portion of the project. The BDAS and MKS transducers were calibrated in-situ within one month prior to each test.

2.3 Water Channel Facility

The NASA Ames FML's water channel facility (figure 2-2) was employed for this effort. It is a closed-circuit, open channel facility. The facility pump runs at a user-selectable variable speed, to control mass flow and hence, test section speed. Flow travels through a honeycomb and three screens into the water channel test section, which

is approximately 40.6 cm wide, 20.3 cm deep, and 2.44 m long. The design velocity in the test section is 3 cm/s, corresponding to a Reynolds Number of approximately 30,000 per meter. The free-stream turbulence level and boundary layer height at the midpoint of the empty test section are approximately 1% and 7.6 cm, respectively. A 7.6 cm tall boundary layer splitter plate was used to control boundary layer thickness; the model was positioned at various locations along the plate to produce different values of boundary layer thickness relative to the height of the model. A more detailed description of the facility can be found in ref. 17.

2.4 Models

Two separate axisymmetric, modified-cosine-shaped, wall-mounted models were employed for this effort. For the wind tunnel tests, a 15.2 cm high (H = 15.2 cm), 45.7 cm base (R = 22.9 cm) diameter machined aluminum model was used. For the water channel tests, a smaller scale (H = 5.1 cm, R = 15.2 cm) sintered nylon version of the wind tunnel model was used. For both models, the height above ground (h) varied with radial distance from the centroid (r) by:

$$h = \frac{H}{2}\left\{cos\left(\pi\frac{r}{R}\right)+1\right\} \quad 0<r<R$$

To minimize chances of model edge damage and personnel injury, the thin, sharp edges of both models were blunted slightly by sanding. Both models were polished to a smooth finish. To facilitate flow visualization sequences, each model was painted flat black. For the FISF sequence, the large model was nickel-plated to a highly reflective smooth mirrored finish, which is required in order to observe and image the fringes. The as-built dimensions of the large model were measured twice with FARO coordinate-measuring arms using first a contact probe and later a laser-scan head. The measurements show up to ± 2.5 mm differences between the design and as-built dimensions. No measurements of the small model were made.

3.0 TEST EQUIPMENT AND PROCEDURES

In general, wind tunnel tests were conducted with the aluminium model mounted to the tunnel floor at the midpoint and centerline of the test section, with the tunnel running at 50 m/s. Exceptions for some measurement techniques are noted in the discussion of the specific technique. For the water channel test, the sintered nylon model was mounted on a splitter plate in the middle of the test section, along the centerline, and the channel was run at 3 cm/s. The model position along the splitter plate was adjusted maintain a model height to boundary layer thickness ratio (δ/h) of three. The measurement techniques used their and test specific equipment are summarized below.

3.1 Dye Injection Flow Visualization (Water Channel)

During water channel flow visualization sequences, a fluorescent dye solution was injected via custom apparatus and illuminated by four UV lamps. Prior to dye flow visualization tests, the model was attached to the water channel floor or splitter plate as appropriate. The water channel was started, and yellow-green dye was injected upstream of the model via a dye injection apparatus, while red dye was injected downstream of the model, within the separated flow region of the model. During some runs a vertical laser sheet was used to illuminate the dye, providing greater detail of the internal flow in the separated region. Photographs and videos were taken of the resultant flow patterns.

3.2 Surface Oil Flow Visualization (Wind Tunnel)

Prior to oil flow visualization tests, the model was painted black and then attached to the wind tunnel floor. The model and the floor downstream of the model were then coated with a filtered mixture of motor oil, artists' pigment, and oleic acid. The tunnel was operated to the desired speed of 50 m/s. The air caused the pigmented oil to flow over the model and floor surface, setting up the various complex patterns. The tunnel was allowed to run at the same velocity for approximately 10 minutes, to ensure that the flow patterns achieved a stable location. The tunnel was stopped, and photographs were taken of the resultant oil patterns from several angles.

3.3 Pressure-Sensitive Paint (Wind Tunnel)

Pressure-sensitive paint measurements were carried out using the "luminescence lifetime" technique [18]. First, the model was coated with FIB-7/PtTFPP paint over a FIB-7/TiO2 basecoat prior to installation in the test section. The painted model was illuminated with four blue (408 nm output) pulsed LED lamps. Both lamps and paint were manufactured by Innovative Scientific Solutions, Inc. The model was viewed with two Roper Scientific CoolSNAP cameras with Kodak KAI4040M CCD sensors, operated in frame accumulation mode. Both cameras and lamps were mounted in the wind tunnel plenum section directly above the model. The lamps illuminated the model through the acrylic ceiling, while the cameras viewed the model through an opening in the ceiling to eliminate noise due to reflections off the windows. Cameras and lamps were reciprocally filtered to eliminate contamination of the PSP images with reflected blue light from the lamps. During operation all other light sources in and around the wind tunnel were switched off to minimize stray light contamination.

The luminescence lifetime technique exploits the fact that the light emitted by PSP in response to illumination has a pressure-dependent decay lifetime; surface pressures can be determined from the ratio of two images taken at different times during the luminescence decay curve. For this test, the LED lamps were operated at a pulse rate of 5000 Hz with a flash duration of 25 µsec. The "gate 1" image was taken coincident with the flash while the "gate 2" image was taken at a 5 µsec delay after the flash. For both images, the gate duration was 25 µsec. Only a few photoelectrons are acquired in each gate, and for this test 3000 individual gates were accumulated to form each data image. The flash and gate timings were chosen to maximize the pressure-sensitivity of the paint signal within the limitations of the camera and lamp equipment.

Relative to other PSP approaches, the luminescence lifetime technique is insensitive to bias errors due to paint photodegradation and especially to temperature variation, which is an especially significant error source in low-speed PSP testing. However cameras which are capable of frame accumulation mode have relatively low full-well capacity and thus higher photon shot noise than conventional cameras. To minimize noise a large number of images were averaged at each test or reference condition. In addition to achieve temperature equilibrium of the model, PSP, and wind, the facility was run for approximately 1.5 hours before acquiring any data. As a result of the extended PSP runs it proved more convenient to take data at 100 and 150 fps (30 and 46 m/s) as opposed to the 50 m/s run speed employed by most other measurement techniques. Once the tunnel had been heat-soaked, 50 wind-on images were acquired. The LED lamps were then turned off and 15 images were acquired to characterize stray light and camera noise. Finally the LED lamps were turned back on, the tunnel was turned off, and 50 wind-off images were immediately acquired to characterize the PSP luminescence lifetime at constant pressure while still retaining the wind-on temperature distribution.

In order to support the PSP measurements, provision was made in the large model for measuring discrete surface pressures at various locations. Twelve separate pressure port holes were drilled in the model and connected via flexible tubing to a PSI 8400 data collection system. Pressure data were acquired along with the PSP images to use as a reference. In addition, discrete pressure data were acquired over a range of wind tunnel speeds independent

of PSP requirements. The wind tunnel was operated at a series of speeds between 0 and 52 m/s in 3 m/s increments, and the data collection routine was operated for each speed, acquiring 6 seconds of pressure data at each speed.

PSP data reduction was carried out as described in reference 18. Pressure taps installed in the model as described above were used to generate an *in* situ correction for the raw PSP data. Black target dots painted on the model were located with a FARO arm, and the known locations of the dots, both on the model and in the PSP images, were used to map the PSP data onto a model surface grid. Once the image data were mapped onto the grid, results from both cameras were averaged in order to further improve signal-to-noise ratio. Even so, the PSP results showed large scatter at these low flow speeds. Scatter between the PSP and pressure tap data indicate an uncertainty for the PSP of ±150 Pa, which for the high speed case corresponds to roughly ±0.1 C_p. While the spatial resolution of PSP is typically limited only by the spatial resolution of the camera, in the FAITH test images were averaged with a 5×5 kernel to reduce noise, thus resulting in a spatial resolution of about 1.2 mm.

3.4 Fringe Imaging for Skin Friction (Wind Tunnel)

FISF exploits the fact that the wedge angle of a thin film of oil with known viscosity can be easily related to local skin friction, and that fringes formed by light interference between the surface of the oil film and the shiny surface of the underlying model can be used as a very sensitive measure of the change in oil film thickness. For the FAITH measurements, the FISF process began with nickel-plating the model to provide a highly reflective and optically uniform surface. (The thickness of the nickel plating and change in surface roughness were considered to have negligible aerodynamic effect.) With the model mounted onto the wind tunnel floor along the test section centerline, oil drops of a known viscosity were applied to the surface. The wind tunnel was then run at the desired test speed of 50 m/s. The wind caused the oil droplets to move in the direction of the surface shear stress. The tunnel was stopped, and a bright extended monochromatic light source was used to illuminate the oil-streaked model, which created an optical fringe pattern on the model. Figure 3-1 shows a sample raw FISF image. The upper right portion of figure 3-1 shows the entire model surface, in an image taken from directly overhead, illuminated in green by the monochromatic light source. Dark lines and white glare spots are due to specular reflections. Images were taken from several slightly different angles to ensure that oil flow fringes could be resolved at all points on the model surface. The lower left portion of figure 3-1 shows a closeup of just one part of the overall image. The fringes can be easily resolved, and the spacing of the fringe pattern is proportional to the thickness of the oil which in turn is proportional to the skin friction. Note that the local flow velocity vector is perpendicular to the fringes, and thus is nearly 45° to the free-stream flow. Fringe spacings determined from the photographs were then mapped onto a 3D surface grid where the actual real-world spacing, and thus the local skin friction coefficient, could be determined. Additional details concerning the FISF technique are found in Ref. 19, which also provides an uncertainty estimate for the technique. For this test the C_f magnitude uncertainty was estimated at ±5% and the direction uncertainty at ±2°. A significant factor in the direction uncertainty is the quality of the photogrammetric transform used map data from the camera image plane to the model surface. Thus the direction uncertainty can vary from point to point on the model. The spatial resolution of the technique is controlled by the typical distance between fringes. For the FAITH experiment the spatial resolution was roughly 2 mm. Test-specific instrumentation used during FISF sequences included silicone-based oil (Dow Corning 200 Fluid), a digital SLR camera with a 546 nm filter, an extended monochromatic light source and data collection and vector processing software running on a PC laptop computer.

3.5 Cobra Probe (Wind Tunnel)

The Cobra probe, made by Turbulent Flow Instrumentation (TFI), Ltd, is a 4 hole pressure probe used to determine unsteady 3D components of velocity at frequencies less than 10 kHz. The Cobra probe employs Honeywell 2.5 kPa transducers to measure flow speeds up to 60 m/s, and has a cone of acceptance of ± 45 deg, centered on the

probe centerline. The probe was connected to the facility data collection and control computer via National Instruments A/D card. Prior to Cobra Probe test sequences, the grid of desired measurement locations was coded into the traverse control module of the data collection system. The wind tunnel was operated at the desired test speed, and the data collection routine was started. The 3-axis traverse, mounted above the test section in the constant pressure plenum moved a single Cobra probe to each of the 3D spatial locations, and acquired 6 seconds of 1250 hz pressure data at each location. Simultaneously, the Cobra probe software computed 3D velocity components for each measurement. The Cobra probe manufacturer provides a calibration for each probe [20]. Under most conditions for this test campaign the Cobra probe velocity accuracy was ±0.5 m/s in magnitude and ±1° in pitch and yaw angle, in flows up to 30% turbulence intensity. The Cobra probe's spatial resolution is limited to the 2.6 mm diameter of the probe head. The choice of data acquisition rate and sampling time were based on previous experience in similar tests in the facility, in which it had been observed that there was negligible frequency content above 600 Hz and that a 6 second sampling time was sufficient for convergence of both the mean velocity data and frequency spectra.

3.6 Particle Image Velocimetry (Wind Tunnel)

The PIV data were acquired using a dual cavity, pulsed Nd:YAG laser with 350 millijoules per pulse and two 11 Megapixel PIV cameras with the frame straddling function. The plane of the laser was projected through the aft test section side wall to a vertical mirror mounted in the aft portion of the test section. This reflected the laser sheet forward, along the centerline of the test section in the vertical stream-wise plane. The mirror was mounted 1.22 m (5.3 hill radii) downstream of the center of the hill. It was 2.5 cm laterally and 15.2 cm high, and is not expected to have had a significant upstream effect on the flow over the model. The two cameras were placed outside the test section, upstream of the model, and viewed the laser light in the forward-scatter mode. The image field of view extended from the top of FAITH to 65 cm downstream, and vertically from the floor to 25 cm. Because of the complexity of changing the position of the laser sheet, off-centerline data planes were acquired by shifting the model laterally in the test section instead. Planes of data were acquired at -5.1, 0 (centerline), 5.1, 7.6, 10.2, 12.1, 15.2, and 17.8 cm. This last data plane corresponds to a shift of the model toward the wind tunnel wall of roughly 0.15 test section widths. Based on pervious observations of blockage effects in this wind tunnel, it was expected that the flow over the model would not be affected.

The system operated at 2 Hz and 4000 samples were acquired for each plane of data. The data were reduced using LaVision DaVis v8 software. The region of interest was processed using 64 x 64 pixel interrogation windows, with 75% overlap. This results in a vector being produced every 2.5 mm in both dimensions along the plane of the laser sheet, based on an interrogation volume of 10×10×0.5 mm. The software uses a grid distortion algorithm that renders velocity gradients that are smaller than the interrogation window (Refs. 21, 22). The 4000 samples were averaged with statistics derived from that average. Prior to PIV sequences, the model and test section interior were painted flat black to minimize unwanted reflections. The seed particles were generated using a pressurized particle generator using 16 Laskin-type nozzles and distributed in the plane of the laser using a distribution rake made with PVC pipe located at the tunnel inlet. The seed was dispensed continuously during the run.

4.0 RESULTS

This section gives a sample of characteristic results from the different measurement techniques. While some comments are made concerning the more obvious flow features revealed, no detailed interpretation of the data is made at this time.

4.1 Water Channel Flow Visualization Tests

The water channel dye flow results provided the first qualitative look at the flow around the model and confirmed that the experiment was producing roughly the expected flow. Figure 4-1 gives a good sense of the overall flow around the model, whose most significant feature is the large separated zone on the downstream side. In figure 4-2, the position of the upstream dye injection apparatus is adjusted so that a line of green dye enters the necklace vortex which forms at the leading edge of the model. Figure 4-3, which was taken by illuminating the wake with a thin sheet of laser light, shows the complicated flow patterns present in the separated wake; this is not simply a one large recirculation zone. Figures 4-1 and 4-3 also serve to qualitatively indicate that the separated flow on the model does reattach and that a region of reverse flow is present. This – per Hunt *et. al.* [1] – would not be the case for a purely laminar upstream flow.

4.2 Wind Tunnel Oil Flow Visualization Tests

Figures 4-4 and 4-5 were taken during the wind tunnel oil flow experiments. They both show the line of separation on the backside of the model, along with the location of reattachment, and even the footprint of a small necklace vortex, which trails back along either side of the base. Figure 4-5 depicts separated, reverse, and low speed separated flow zones via various pigmented oils. Of particular note is the highly symmetrical nature of the flow field and the presence of the two foci, typical of a 3-D separation line culmination.

4.3 Wind Tunnel Pressure-Sensitive Paint (PSP) Tests

Figure 4-6 shows an overhead view of the PSP results for the higher speed (46 m/s) case. Data from both cameras have been projected onto a 3D surface grid, averaged on the grid, and then a synthetic view from directly overhead was generated. The surface pressure coefficient varies from about 0.25 in the attachment region on the upstream slope to -1.5 just before the top of the hill where maximum flow acceleration occurs. Figure 4-7 compares the oil flow and PSP data for the high speed (PSP at 46 m/s, oil flow at 50 m/s) case. Flow attachment is clearly seen to occur at the point of maximum pressure, and separation is clearly located in the zone of adverse pressure gradient on the downstream side of the model. However more subtle features of the oil flow images, such as nodes and secondary separation and attachment points, are not resolved by the PSP data. PSP results for the low speed (30 m/s) case show the same general trends as for the high speed case. However the lower speed PSP data are noisier and flow features are more difficult to resolve.

4.4 Wind Tunnel Fringe Imaging Skin Friction (FISF) Tests

Skin friction values derived from FISF are shown in figure 4-7, which shows skin friction vectors and is colored according to the local skin friction magnitude. Vectors are not apparent near the upstream attachment region or in the separated zone downstream. Data were obtained in these regions; the vectors are simply too small to show up well in the figure. One item of interest are the two local skin friction coefficient maxima, approximately halfway up the model, on either side of the model centerline. No simple physical explanation for this phenomenon has occurred to the authors, however a simulation by Rodio *et.al.* [25] using the Spalart-Allmaras model appears to show a similar bi-lobed arrangement of skin friction maxima (Rodio *et. al.* fig. 7).

4.5 Wind Tunnel Cobra Probe Tests

Figure 4-9 shows sample velocity measurements from the Cobra probe. In the figure, mean streamwise velocity is plotted versus vertical distance from the wind tunnel floor, on the centerline of the wind tunnel, at different distances upstream of the model. Velocity profiles were obtained at locations varying from 1.02 to 2.44 model

radii (*x/R*) upstream from the center of the model. (Thus *x/R* = -1.02 corresponds to the leading edge of the model.) A detectable influence of the model can be seen even fairly far upstream, at *x/R* = -2.44. However note that this location is still far behind the entrance to the test section which is located at *x/R* = -6.67. The mean flow data in figure 4-9 represent only a small fraction of the Cobra probe data which were acquired. Figure 4-10 gives a better idea of the total data volume, showing mean streamwise velocity at six cross-flow planes both upstream and downstream of the model. The data show the velocity deficit both ahead of and behind the model. Also, distinct velocity deficits corresponding to the necklace vortices can be seen in the downstream data planes. The flow appears to be bilaterally asymmetric, with a stronger velocity deficit apparent to the right of centerline. The reason for this asymmetry is unclear.

4.6 Wind Tunnel Particle Image Velocimetry (PIV) Tests

Figures 4-11 through 4-14 depict results of the PIV testing for the centerline plane (y = 0.0) of data. Figure 4-11 depicts the mean downstream velocity magnitude in color, with velocity vectors superimposed. Note the large region of separated and reversed flow downstream of the hill. Because the large number of vectors can tend to obscure color magnitudes, the remaining figures are shown with vectors suppressed. Figures 4-12 and 4-13 depict the unsteady streamwise velocity component (u') and the primary Reynolds Stress (u'v') component, respectively. Figure 4-14 depicts the variation of Turbulent Kinetic Energy (TKE). As expected, the maximum levels of the Reynolds stresses occur in the separated shear layer.

5.0 CONCLUDING REMARKS

5.1 Summary

A series of experiments, using both qualitative and quantitative techniques, were conducted at NASA Ames Research Center's Fluid Mechanics Lab (FML) to characterize both surface and flow field characteristics of an axisymmetric, modified-cosine-shaped, wall-mounted (FAITH) hill. The aim of the tests was to produce a well-documented dataset which would be useful in validating CFD codes. The dataset includes the following items:

1. Off-body flow visualization results (water channel).
2. On-body measurements of surface pressure (using PSP and pressure taps), skin friction (using FISF), and surface flow visualization (using oil flow).
3. Off-body velocity measurements as follows:
    a. Time-resolved three-component velocity measurements in both streamwise and cross-stream planes, upstream and downstream of the model using a Cobra probe.
    b. Three-component velocity and turbulence statistics measurements in streamwise planes behind the model using PIV.
4. Uncertainty estimates for the experimental measurements.
5. As-built CAD geometry for the wind tunnel model.
6. Spot-checked CAD geometry for the wind tunnel.

This report summarizes the experimental set-up, techniques used, and data acquired, and also describes some details of the dataset that is being constructed for use by other researchers, especially the CFD community. Subsequent reports will discuss the data and their interpretation in more detail. Some theoretical and computational studies have already been completed using this dataset as a reference. Tobak [23] has made an analysis of the topological aspects of the flow as revealed by the oil flow visualization, attempting to determine if the flow around

the FAITH model could be mapped to the flow around a hemispherical bump, which has identical topological features. Olsen *et. al.* [24] used the FAITH dataset as part of work to validate new Reynolds stress models in OVERFLOW. Rodio *et. al.* [25] used the Wilcox 2006 stress-ω and Spalart-Allmaras models implemented in CFL3D to predict the flow around FAITH with "fair" agreement for the mean properties. In addition further experimental studies have been made of the FAITH model shape by other researchers. Husen *et. al.* [26] describe an experiment in which a global luminescent oil-film skin friction meter is developed and used for measurements on a cosine hill similar to FAITH.

5.2 Experiment and CFD Comparisons

Ideally in any CFD/experiment comparison the CFD simulation will reproduce the boundary conditions of the experiment to the greatest degree practical. In the case of comparisons with the FAITH dataset, the authors believe there are two ways this may be achieved. First, the FML Test Cell #2 wind tunnel geometry is specified well enough that the entire indraft wind tunnel can be simulated. Second, the upstream and downstream Cobra probe data planes can be used to establish inflow and outflow boundary conditions. Another factor in experiment/CFD comparisons is the spatial and temporal filtering of CFD data to match that of the experimental results, which are always obtained using measurement techniques with finite spatial resolution and time response. CFD data should be spatially averaged over lengths scales equal to the spatial resolution of the experimental techniques. These scales vary by technique and are given in section 3. With regard to temporal filtering, one issue which arises is that the PSP, FISF, and PIV data were all obtained over time scales of several minutes. However individual Cobra probe measurements show that mean velocity measurements converge after roughly 6 seconds and it is recommended that mean CFD results be averaged over at least this time.

5.3 Issues with Multiple Experimental Techniques for CFD Validation

One important goal of the FAITH project was to bring to bear a number of different experimental techniques on the same flow. This is an inherently complex task. The different experimental techniques all have their own, often incompatible, requirements for model surface treatment, optical access, and measurement time. In FAITH, most of these problems were solved by allocating each measurement technique its own time period in the wind tunnel schedule. This had the added advantage of allowing results from one technique to inform the planning of the following experiments. However this approach also allows a situation where details of the tunnel operation may vary slightly (*e.g.* exact flow speed, pre-experiment heat soak periods) in order to optimize conditions for individual measurement techniques. Also, because the FAITH tests were conducted over a span of several months, the issue of facility and installation repeatability becomes a factor. The Test Cell #2 wind tunnel maintains a periodic calibration process for the instruments which control tunnel speed setting. But in general measurements of the FAITH flow with the same technique were not repeated across multiple installations of the model or large spans of time. The decision to forgo explicit statistical process control was based on limitations on available resources and the authors' engineering judgment about long term stability of the Test Cell #2 wind tunnel. However in further FAITH experiments this would be a useful topic to address.

6.0 ACKNOWLEDGMENTS

This work was supported by the NASA Fundamental Aero Program (Subsonic Fixed Wing Project), with Dr. Mike Rogers, as Technical Lead for Efficient Aerodynamics. The authors also wish to thank Dennis Acosta, Louise Walker, Barry Porter, Laura Kushner, Ted Garbeff, and Murray Tobak, all of NASA Ames Research Center, as well as Summer Interns, Katy Swanson (Rose-Hulman Institute of Technology) and Rob Bulmann (California Polytechnic University – San Luis Obispo) for their assistance in the completion of this project.

7.0 REFERENCES

[1] Hunt, J.C.R., Abell, C.J., Peterka, J.A., Woo, H., "Kinematical Studies of the flows around free or surface-mounted obstacles; applying topology to flow visualization," J. Fluid Mech. 86 (1), 1977, pages 179–200.

[2] Hunt, J. C. R. & Snyder, W. H., "Experiments on stably and neutrally stratified flow over a model three-dimensional hill," J. Fluid Mech. 96, 1980, pages 671–704.

[3] Ishihara, T., Hibi, K., Oikawa, S., "A wind tunnel study of turbulent flow over a three-dimensional steep hill," J. Wind Eng. Indus. Aerodyn. 83, 1999, pages 95–107.

[4] Apsley, D. D. & Castro, I. P. "Flow and dispersion over hills: comparison between numerical predictions and experimental data," J. Wind Eng Ind. Aerodyn. 67–68, 1997, pages 375–386.

[5] Willits, S.M. & Boger, D.A., "Measured and predicted flows behind a protuberance mounted on a flat plate," Applied Research Laboratory Report, Penn State Univ., State College, PA, August 30, 1999.

[6] Simpson, R.L., Long, C.H., and Byun, G. "Study of Vortical Separation From an Axisymmetric Hill," International Journal of Heat and Fluid Flow 23, 2002, pages 582–591.

[7] Byun, G., Simpson, R. L. & Long, C. H. "Study of vortical separation from three-dimensional symmetric bumps," AIAA J. 42 (4), 2004, pages 754–765.

[8] Byun, G. & Simpson, R. L. "Structure of three-dimensional separated flow on an axisymmetric bump", AIAA J. 44 (5), 2006, pages 999–1008.

[9] Byun, G. and Simpson, RL., "Surface-Pressure Fluctuations from Separated Flow over an Axisymmetric Bump," AIAA Journal Vol. 48, No. 10, October 2010.

[10] Thiele, F. & Jakirli, S., "12TH ERCOFTAC/IAHR/COST Workshop on Refined Turbulence Modelling," Technical University of Berlin, Germany, October 12-13, 2006.

[11] Patel, N. and Menon, S.,"Structure of flow separation and reattachment behind an axisymmetric hill," Journal of Turbulence, Volume 8, 2007.

[12] Persson, T., Liefvendahl, M., Bensow, R.E., & Fureby, C., "Numerical investigation of the flow over an axisymmetric hill using LES, DES, and RANS," Journal of Turbulence, Volume 7, 2006.

[13] Krajnovic, S., "Large Eddy Simulation of the Flow Over a Three-Dimensional Hill" Flow, Turbulence and Combustion Volume 81, Numbers 1-2, 2008, pages 189-204.

[14] Garcia-Villalba, M, Li, N., Rodi, W., and Leschziner, M.A., "Large-eddy simulation of separated flow over a three-dimensional axisymmetric hill", J. Fluid Mech. vol. 627, 2009, pp. 55–96.

[15] Bell, J.H., Heineck, J.T., Zilliac, G., Mehta, R.D., Long, K.R., "Surface and Flow Field Measurements on the FAITH Hill Model" 50th AIAA Aerospace Science Meeting, January 9-12, 2012, Nashville, TN, AIAA 2012-0704

[16] "SAFE OPERATING PROCEDURES (SOP) FOR THE NASA AMES FLUID MECHANICS LAB (FML) 48" x 32" INDRAFT WIND TUNNEL" Revision D, Feb 20, 2011. AOX-2010-006

[17] "SAFE OPERATING PROCEDURES (SOP) FOR THE NASA AMES FLUID MECHANICS LAB (FML) WATER CHANNEL" Revision 2, Feb 27, 2011. AOX-2010-008

[18] Bell, J.H., Schairer, E.T., Hand, L.A. and Mehta, R.D. "Surface Pressure Measurements Using Luminescent Coating," Annual Review of Fluid Mechanics, Vol. 33, pp. 155-206, 2001.

[19] Zilliac, G.G., "The Fringe Imaging Skin Friction Technique PC Application V5.0 User's Manual," NASA TM-2010-216391, July. 2010.

[20] Mousley, Peter D., "Cobra Probe User Guide," Turbulent Flow Instrumentation Pty Ltd. 2001.

[21] Scarano, F. "Iterative image deformation methods in PIV," Review article, Measurement Science and Technology, 13, 2002.

[22] Baresh, S.J. "Comparison of PIV data using multiple configurations and processing techniques," Experiments In Fluids, DOI 10.1007/s00348-009-0685-7, 29 May, 2009.

[23] Tobak, M. "Topological Aspects of the FAITH Experiment", Invited Presentation to the AIAA Joint Working Group on Fluid Dynamics Challenges in Flight Dynamics

[24] Olsen, M.E., Lillard, R.P., Murman, S.M. "Prediction of Large Separations with Reynolds Stress Models", 21st AIAA Computational Fluid Dynamics Conference, June 24-27, 2013, San Diego, CA, AIAA 2013-2720

[25] Rodio, J.J., Patton, C.H., Xiao, X., Hassan, H.A., "Simulation of the FAITH Hill Experiment using a Reynolds Stress Model", 44th AIAA Fluid Dynamics Conference, June 16-20, 2014, Atlanta, GA, AIAA 2014-2210

[26] Husen, N., Woodiga, S., Liu, T., Sullivan, J.P., "Global Luminescent Oil-film Skin-Friction Meter Generalized to Three-Dimensional Geometry and Applied to FAITH Hill", AIAA SciTech, January 13-17, 2014, National Harbor, Md, AIAA 2014-1237

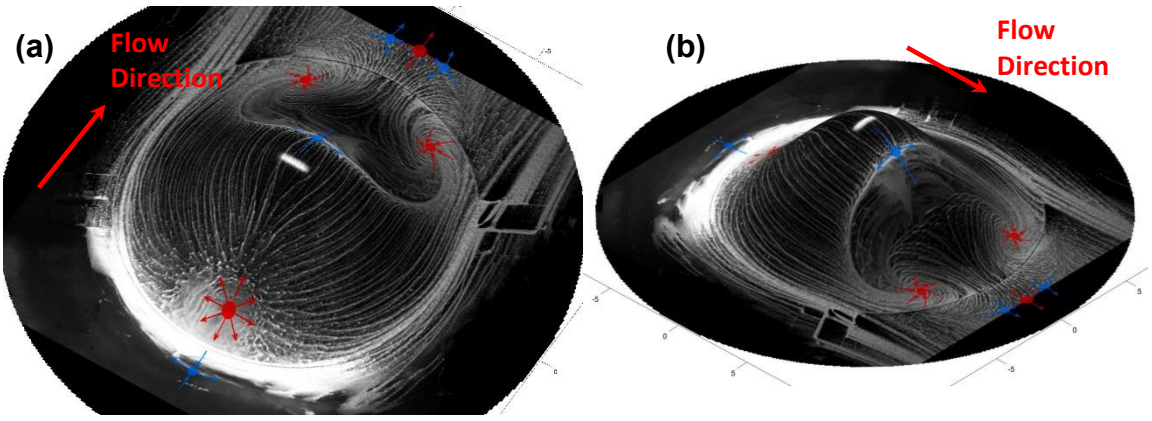

Figure 1-1: Surface oil flow views of a wall-mounted axisymmetric hill from upstream (a) and downstream (b). Topological features are marked including nodes (red) and saddle points (blue).

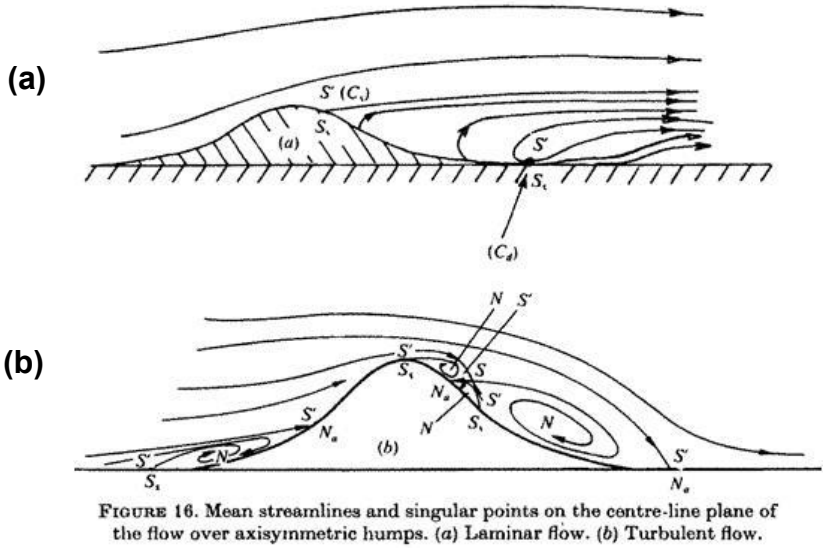

FIGURE 16. Mean streamlines and singular points on the centre-line plane of the flow over axisymmetric humps. (*a*) Laminar flow. (*b*) Turbulent flow.

Figure 1-2: Cartoon showing flow over a wall-mounted axisymmetric hill for laminar (a) and turbulent (b) condition. Taken from Hunt *et. al.* (Reference 1).

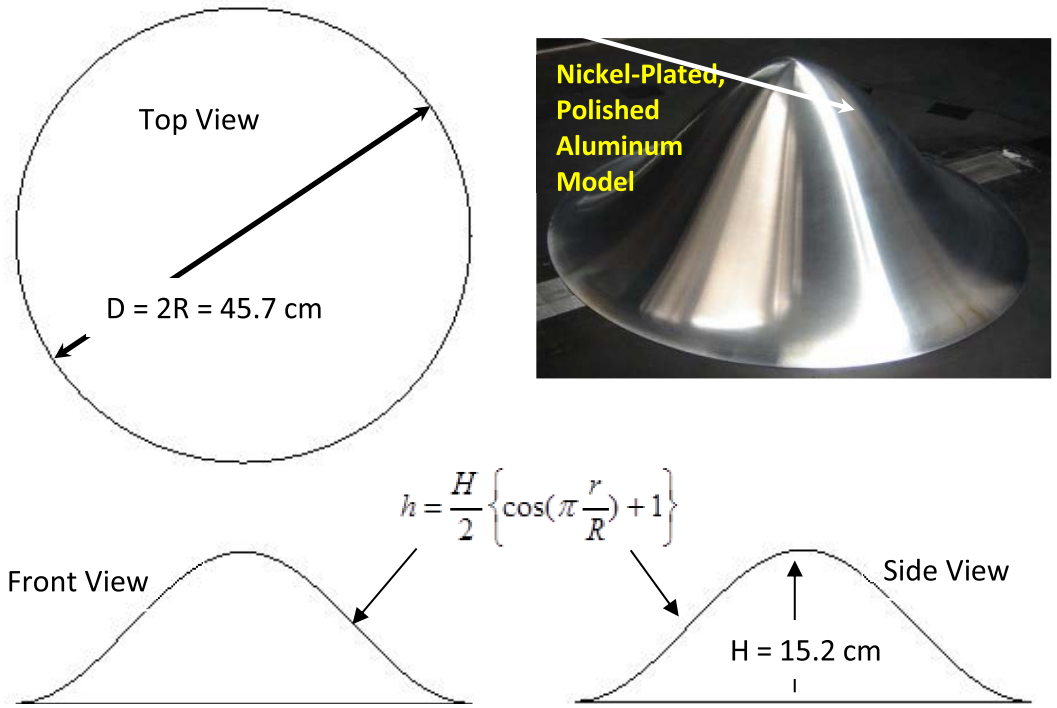

Figure 1-3: Views of aluminum wind tunnel model with dimensions and generating equation.

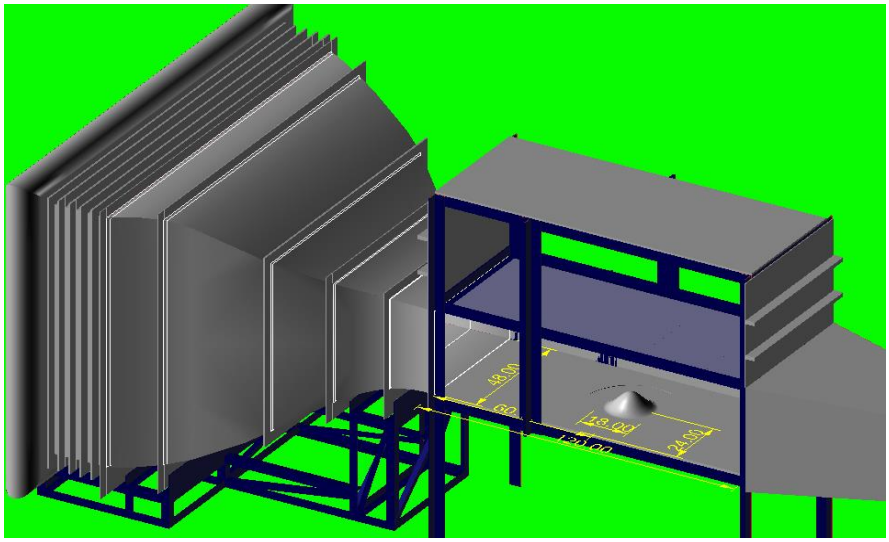

Figure 2-1: View of FML Test Cell #2 from CAD model, showing FAITH model in test section.

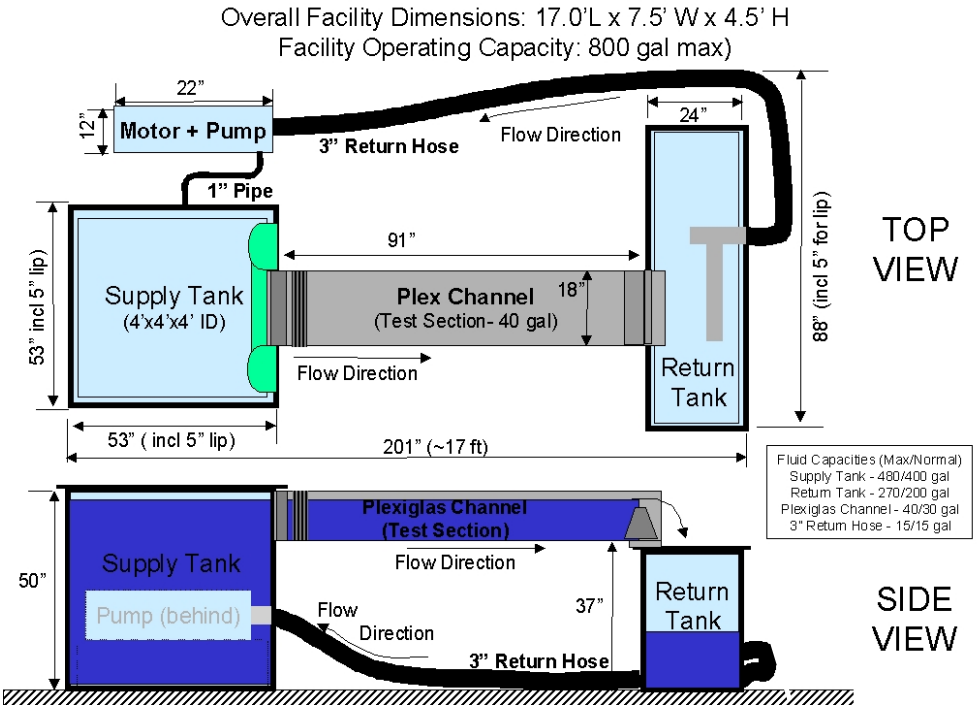

Figure 2-2: Details of NASA Ames Fluid Mechanics Laboratory water channel.

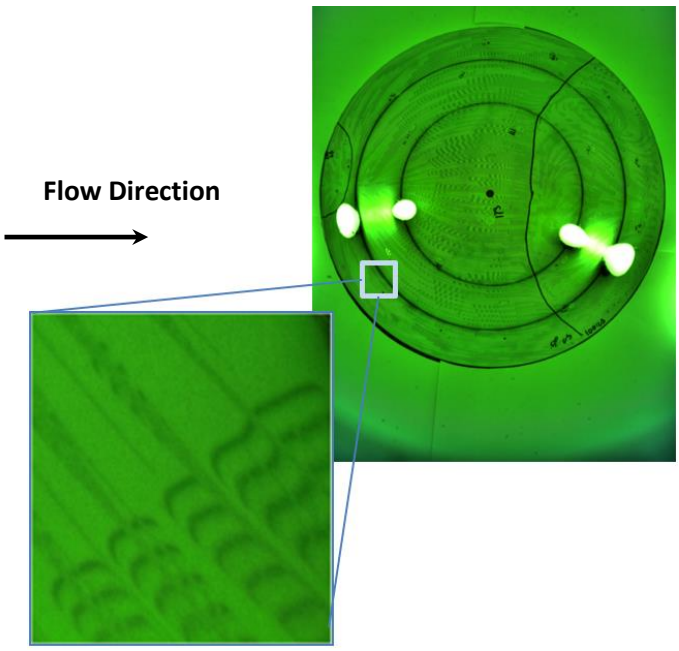

Figure 3-1: FISF raw images showing interferograms of surface oil flow.

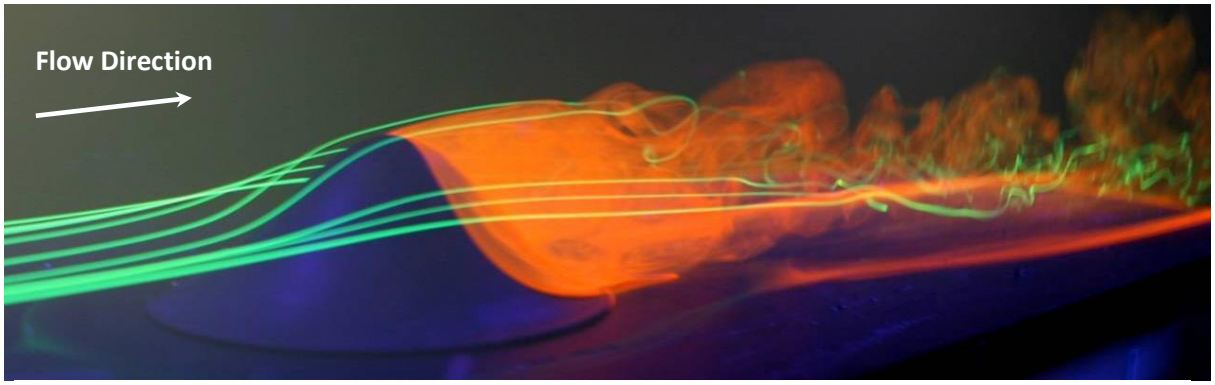

Figure 4-1: Water channel flow visualization (view from upstream). Green dye is injected from horizontally-mounted rake upstream of model and red dye is injected from surface port downstream.

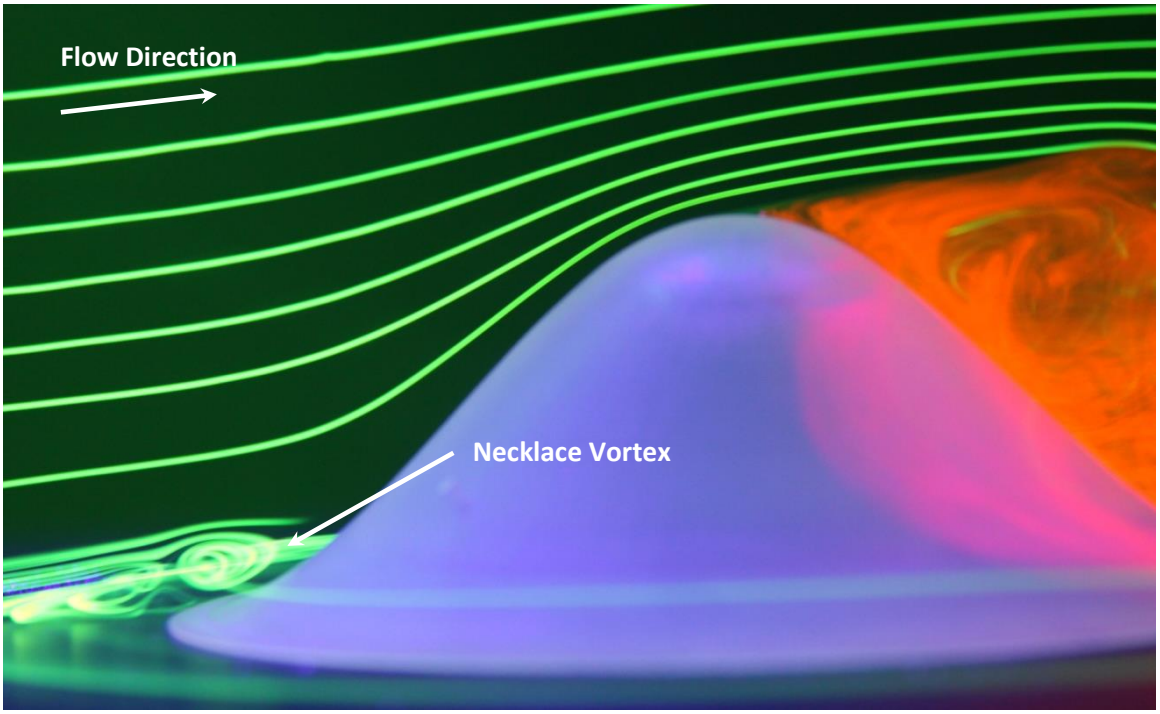

Figure 4-2: Water channel flow visualization (showing upstream necklace vortex). Green dye injection rake is now oriented vertically.

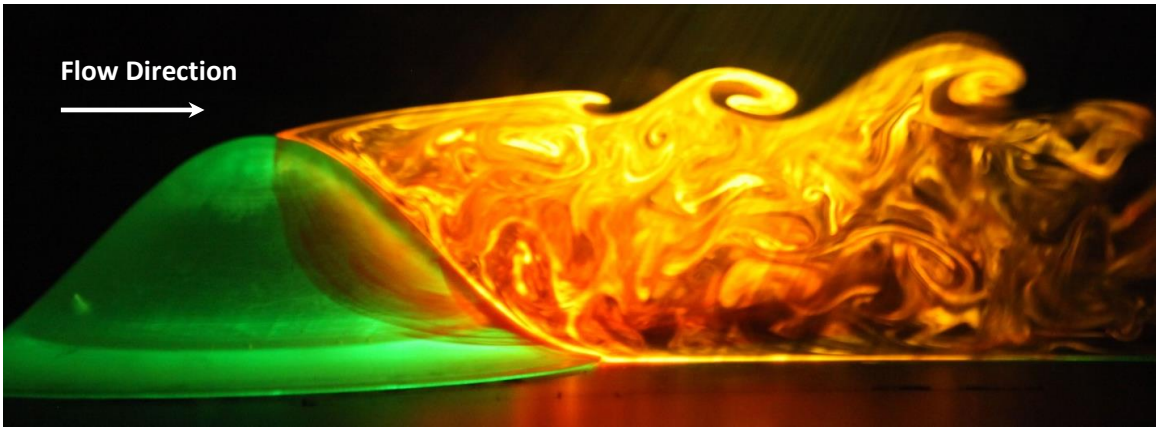

Figure 4-3: Water channel flow visualization (flow centerline illuminated by laser sheet).

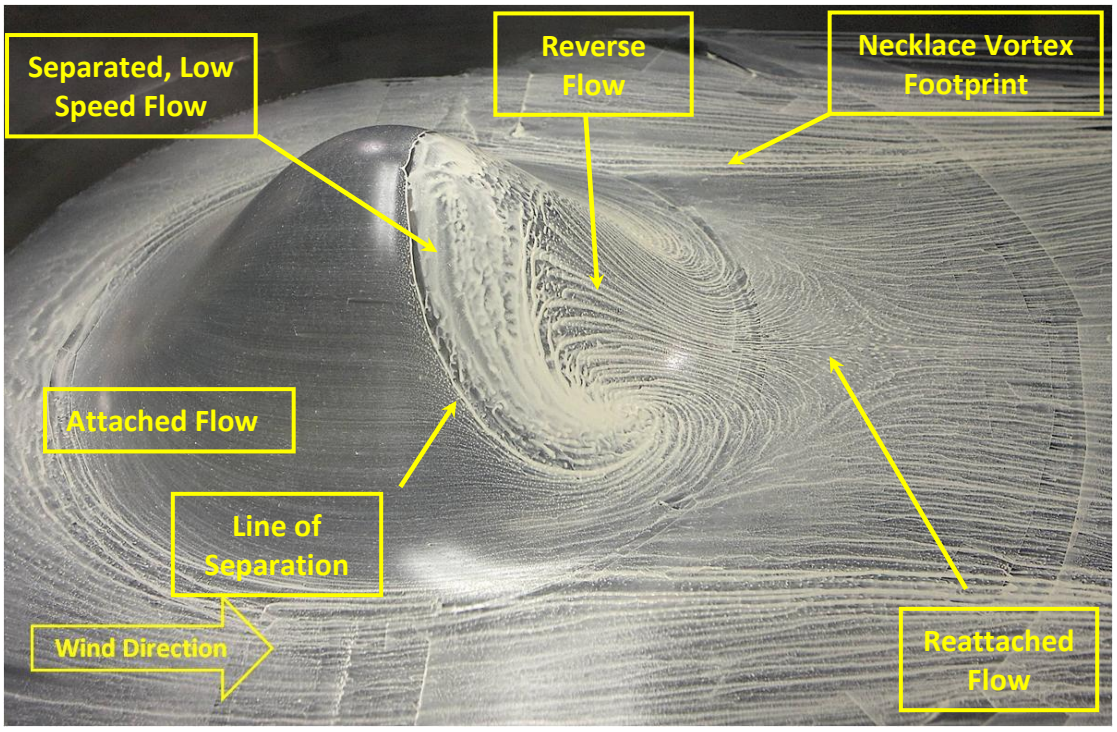

Figure 4-4: Wind tunnel surface oil flow visualization with flow features annotated.

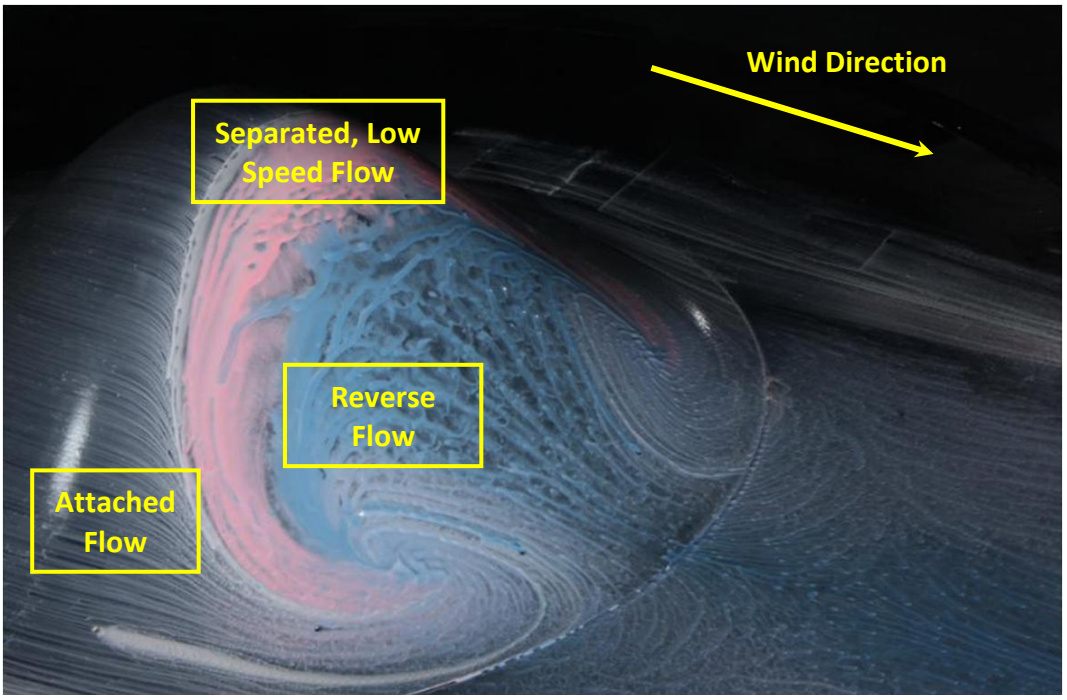

Figure 4-5: Surface oil flow visualization showing downstream side of model with regions of attached, separated, and reverse flow treated with white, red, and blue colored oil, respectively.

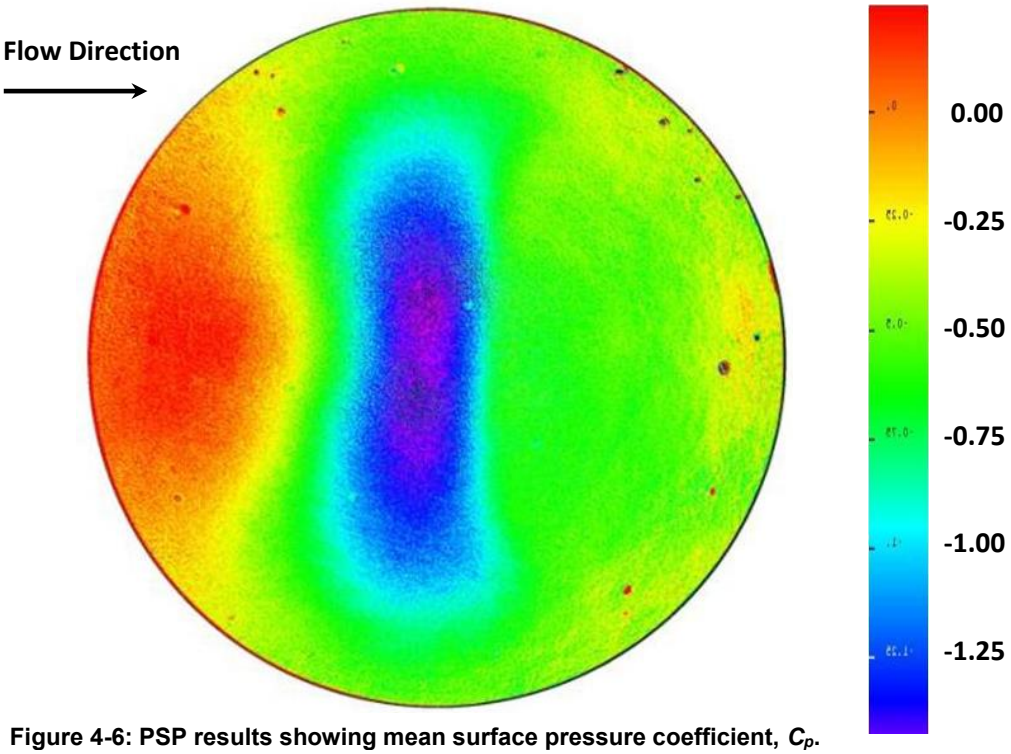

Figure 4-6: PSP results showing mean surface pressure coefficient, C_p.

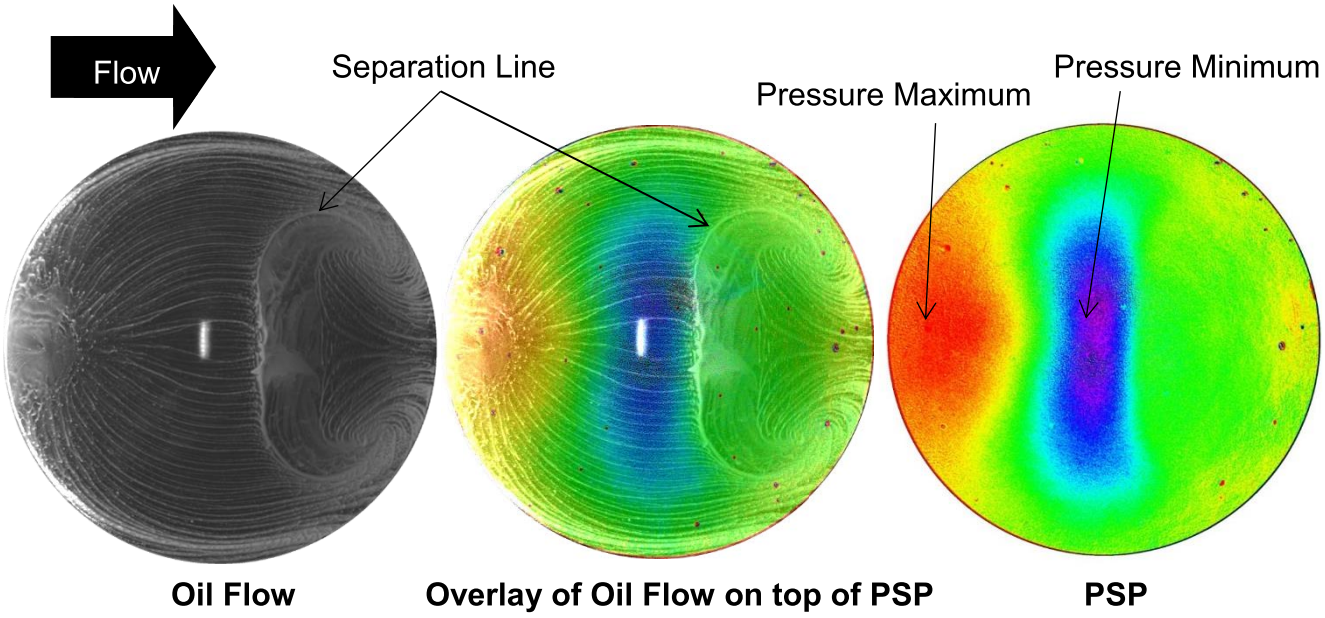

Figure 4-7: PSP and oil flow results overlaid to show surface pressure and flow topology features.

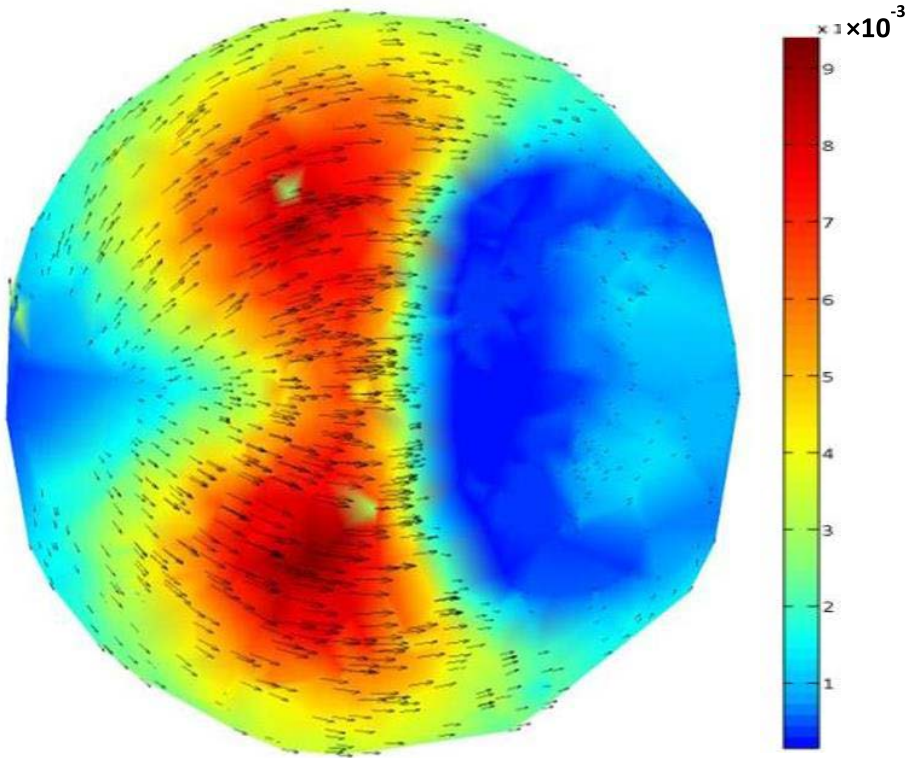

Figure 4-8: Skin friction coefficient (C_f) direction (vectors) and magnitude (colors) from FISF.

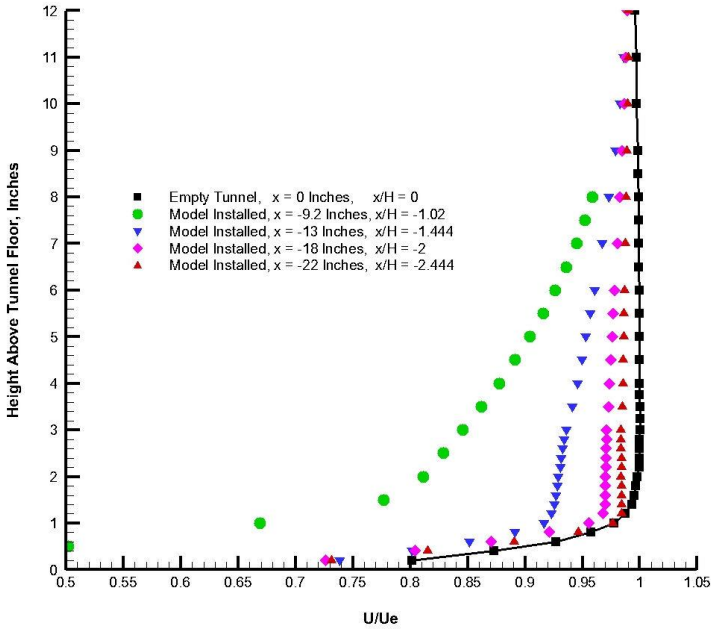

Figure 4-9: Cobra probe mean streamwise velocity ($\bar{u}$) profiles along centerline (z = 0).

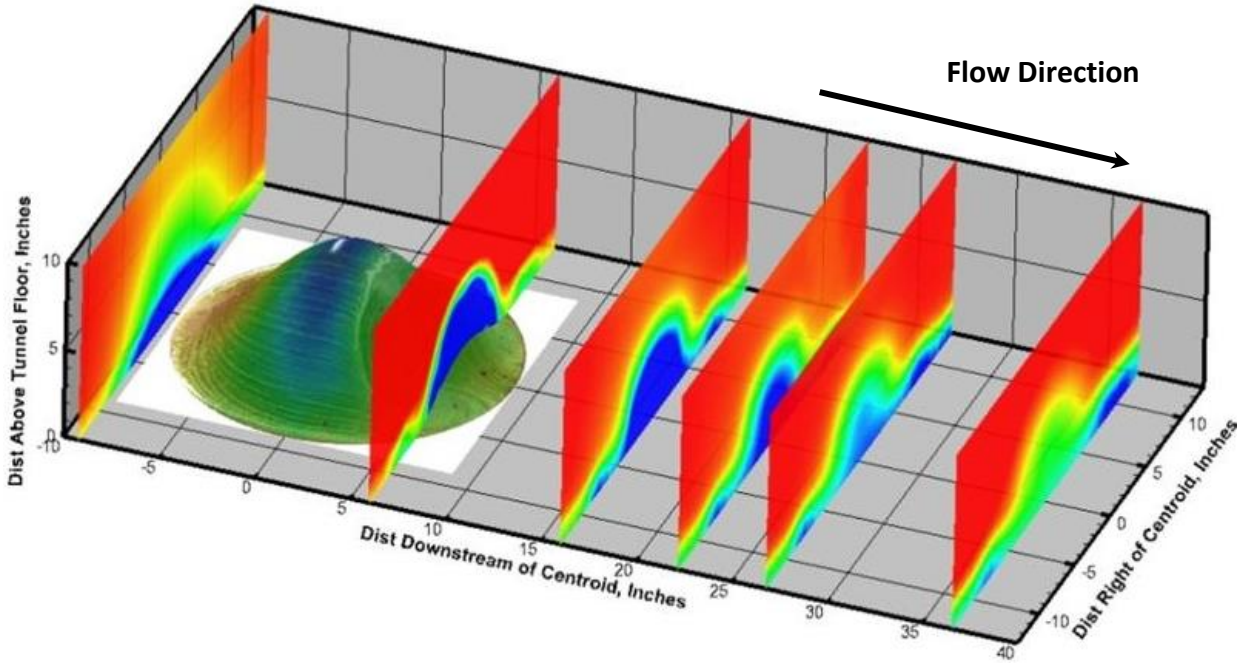

Figure 4-10: Combined data: PSP, oil flow, and Cobra probe mean streamwise velocity ($\bar{u}$) measurements.

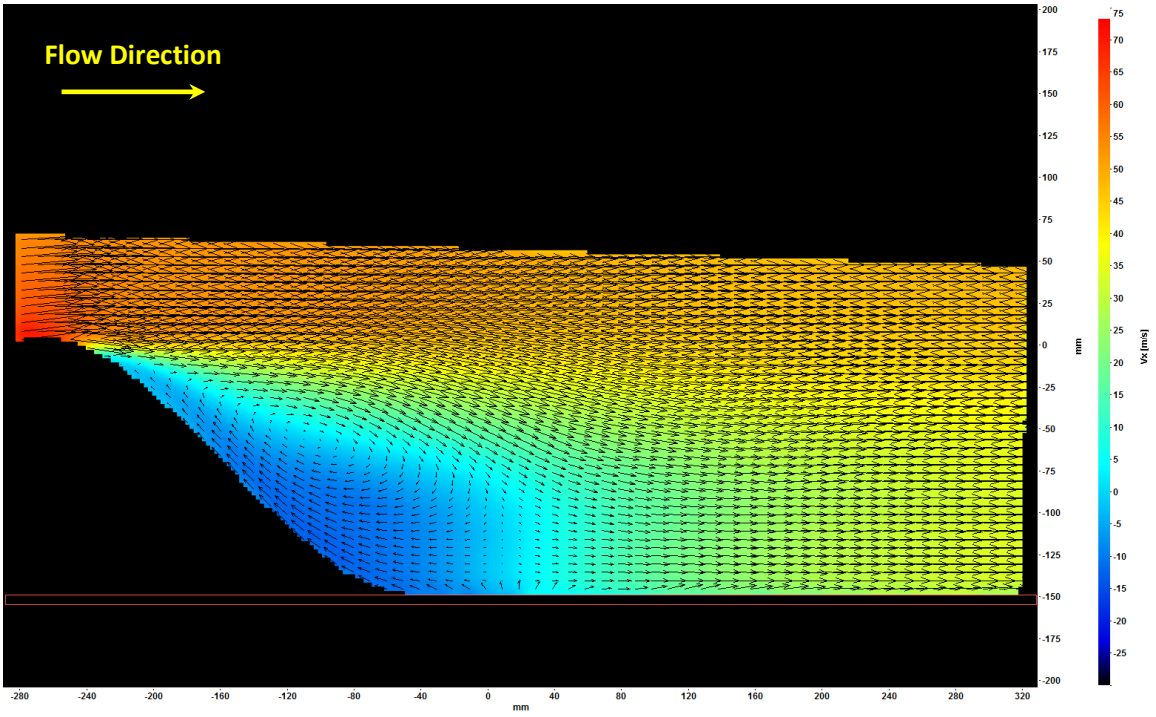

Figure 4-11: PIV data showing time-averaged streamwise velocity magnitude ($\bar{u}$) in colors and time-averaged in-plane velocity as vectors.

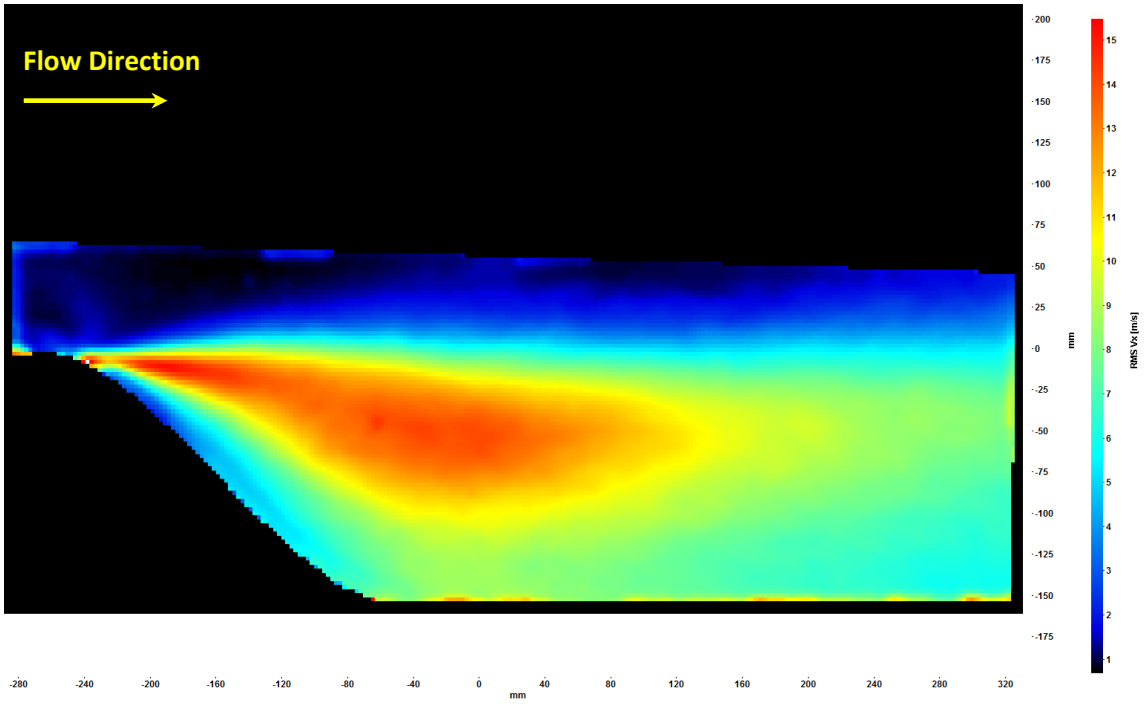

Figure 4-12: PIV unsteady downstream velocity data, $\sqrt{\overline{(u')^2}}$.

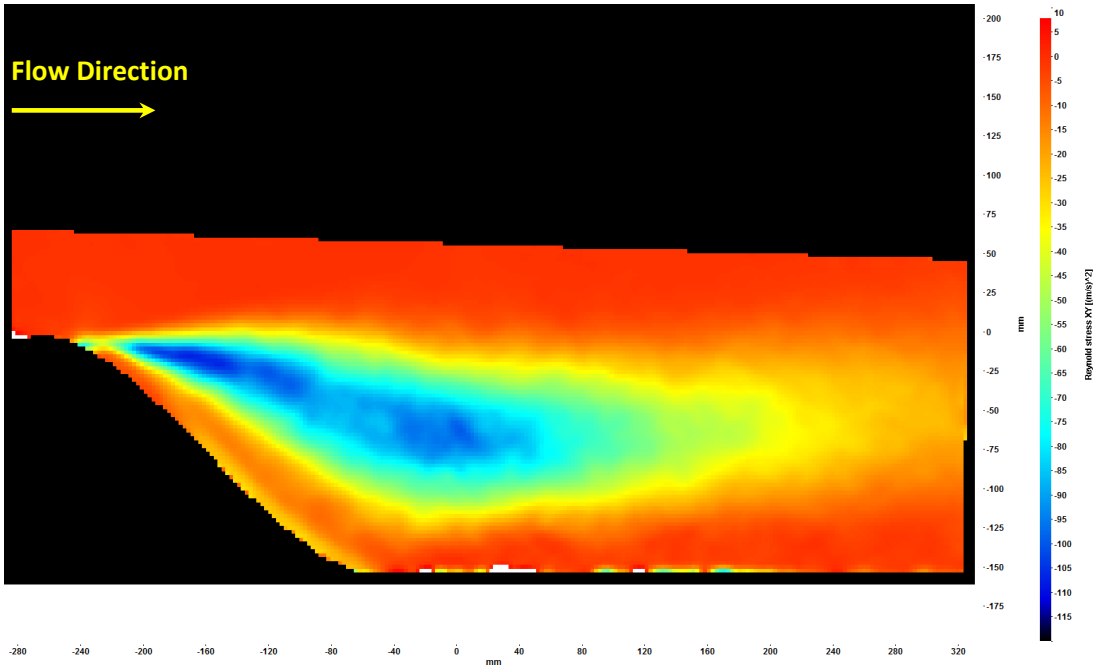

Figure 4-13: PIV Primary Reynolds Stress data ($\overline{u'v'}$).

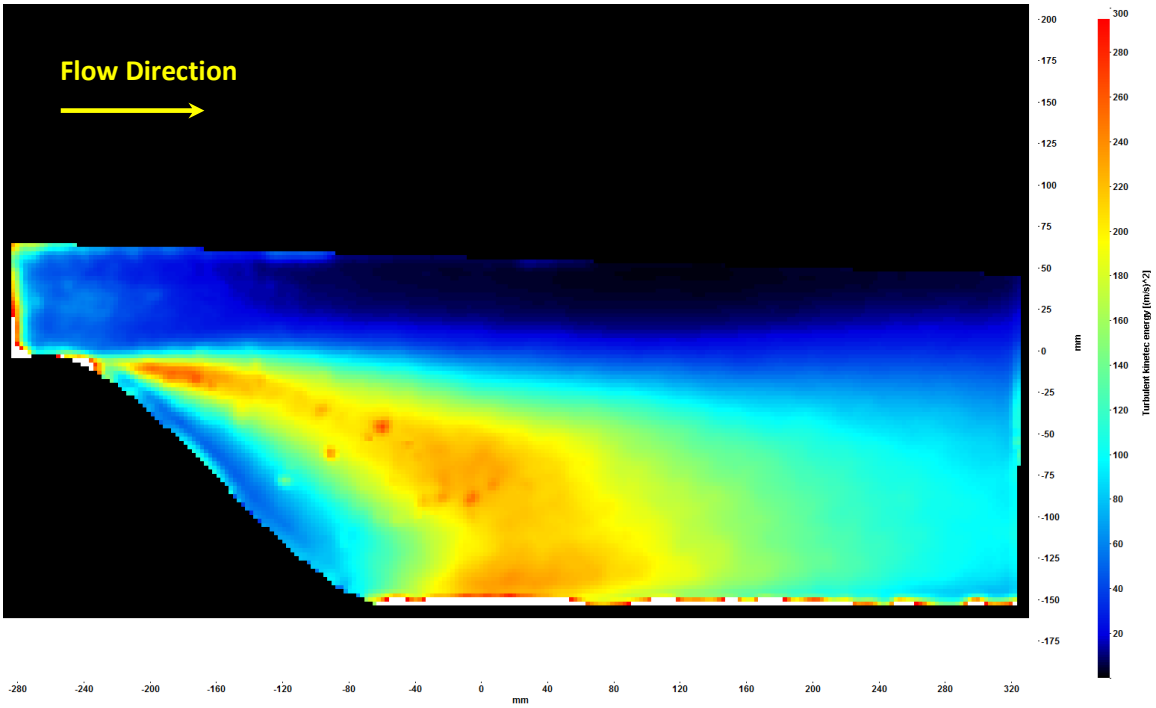

Figure 4-14: PIV data Turbulent Kinetic Energy [$\overline{(u')^2} + \overline{(v')^2} + \overline{(w')^2}$]/2.